minerals

Article

REE and Y Mineralogy of the Krudum Granite Body (Saxothuringian Zone)

Miloš René

Institute of Rock Structure and Mechanics, v.v.i., Academy of Sciences of the Czech Republic, V Holešovičkách 41, 182 09 Prague 8, Czech Republic; rene@irsm.cas.cz; Tel.: +420-266-009-228

Received: 9 April 2018; Accepted: 2 July 2018; Published: 5 July 2018

Abstract: The Krudum granite body comprises highly fractionated granitic rocks ranging from medium-F biotite granites to high-F, high-P_2O_5 Li-mica granites. This unique assemblage is an ideal site to continue recent efforts in petrology to characterize the role of zircon, monazite, and xenotime as hosts to rare earth elements (REEs). The granitic rocks of the Krudum body analyzed in this study were found to contain variable concentrations of monazite and zircon, while xenotime was only found in the high-F, high-P_2O_5 Li-mica granites and in the alkali-feldspar syenites of the Vysoký Kámen stock. Intermediate trends between cheralite and huttonite substitutions are characteristic for analyzed monazite grains from all magmatic suites. The highest concentration of cheralite was found in monazite from the alkali-feldspar syenites (up to 69.3 mol %). The proportion of YPO_4 in analyzed xenotime grains ranges from 71 to 84 mol %. Xenotime grains are commonly enriched in heavy rare earth elements (HREEs; 9.3–19.5 wt % $HREE_2O_3$) and thorite-coffinite and cheralite exchange was observed. Some xenotime analyses return low totals, suggesting their hydration during post-magmatic alterations. Analyzed zircon from granite suites of the Krudum granite body contains moderate Hf concentrations (1.0–4.7 wt % HfO_2; 0.010–0.047 apfu Hf). The highest concentrations of HfO_2 were found in zircon from the high-F, high-P_2O_5 Li-mica granites (1.2–4.7 wt % HfO_2). Analyzed zircon grains from the high-F, high-P_2O_5 Li-mica granites and alkali-feldspar syenites are enriched in P (up to 8.29 wt % P_2O_5; 0.24 apfu P), Al (0.02–2.0 wt % Al_2O_3; 0.00–0.08 apfu Al), Ca (up to 3.9 wt % CaO; 0.14 apfu Ca), Y (up to 5.5 wt % Y_2O_3; 0.10 apfu Y), and Sc (up to 1.17 wt % Sc_2O_3; 0.03 apfu Sc). Zircon grains from the high-F, high-P_2O_5 Li-mica granites were sometimes hydrated and fluorized. The concentrations of F in zircon from partly greisenised high-F, high-P_2O_5 Li-mica granites reached up to 1.2 wt % (0.26 apfu F).

Keywords: monazite; xenotime; zircon; granite; Bohemian Massif; Horní Slavkov; Karlovy Vary

1. Introduction

In the last ten years, several studies have emphasized the role of monazite, xenotime, and zircon as major hosts for rare earth elements (REE) and Y in granites [1–9]. However, several factors controlling the composition of the above mentioned accessory minerals remain unclear. To expand on this knowledge, unique assemblages of variable fractionated granites in the Karlovy Vary pluton were selected for further analyses on these minerals.

The presented study concentrates on petrological and geochemical observations connected to the occurrence of monazite, xenotime, and zircon in compositionally different granitic rock types of the Krudum granite body. This granite body is a subsidiary intrusion of the Karlovy Vary pluton in the Slavkovský Les Mts.

2. Geological Setting

The Karlovy Vary pluton forms the southern edge of the Western Erzgebirge pluton that is part of the Variscan Krušné Hory/Erzgebirge batholith in the western part of the Bohemian Massif [10–12]. This batholith consists of three individual plutons: Western, Middle and Eastern, each representing an assembly of shallowly emplaced granite units about 6–10 km paleodepth, with a maximum preserved vertical thickness of the pluton 10–13 km below the present surface level [12,13]. The batholith belongs to one coherent and cogenetic, ca. 400 km long plutonic megastructure of the Saxo-Danubian Granite Belt [14].

Geochemically, five groups of granites were previously distinguished in the Krušné Hory/Erzgebirge batholith: (i) low-F biotite granites, (ii) low-F two-mica granites, (iii) high-F, high P_2O_5 Li-mica granites, (iv) high-F, low-P_2O_5 Li-mica granites, and (v) medium-F biotite granites [10,11]. However, the above type (iii) has been divided in the current study as high-F, high-P_2O_5 Li-mica granites (iii), and muscovite-biotite high-F, high-P_2O_5 granites (vi). Finally, a new discovery in this study was a quartz-free alkali-feldspar syenite (vii), which forms a distinct separate part of the Vysoký Kámen stock. The Western Krušné Hory/Erzgebirge pluton is interpreted as a sequence of separately emplaced magma batches or an assemblage of several magmatic pulses, emplaced more or less contemporaneously [10,11,15]. The outcrops of this pluton could be divided into the Nejdek–Eibenstock and Karlovy Vary plutons [12,16].

All granitic rocks of the Karlovy Vary pluton were interpreted according their structural setting with respect to the Variscan collision as post-collisional intrusions [10]. Various geochronology methods imply that all these granitic rocks formed between 327 and 318 Ma [10,11,15].

The Krudum granite body (KGB, ca. 50 km^2) on the southwestern margin of the Karlovy Vary pluton (KVP) shows a concentric structure (Figure 1).

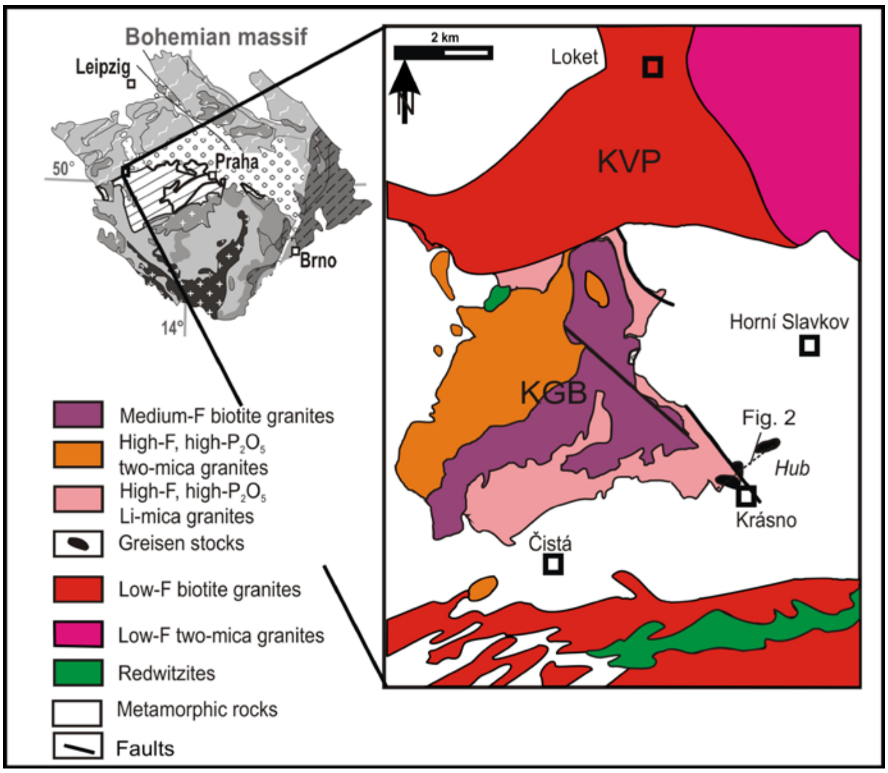

Figure 1. Schematic geological map of the Krudum granite body modified after [17].

Porphyritic medium-F biotite granites, surrounded to the NW by younger, high-F, high-P_2O_5 topaz-bearing muscovite-biotite granites, form its center. The youngest, high-F, high-P_2O_5 Li-mica granite forms the outermost shell [17]. The inner structure of the south-eastern edge of the KGB, partly overlain by metamorphic rocks of the Slavkov crystalline unit, is well stratified, comprising variable greisenised high-F, high-P_2O_5 Li-mica granites occurring also in the Hub, and Schnöd greisen stocks hosting the world-famous Sn-W-Nb-Ta-Li mineralization of the Horní Slavkov-Krásno ore district [18–22] (Figure 2).

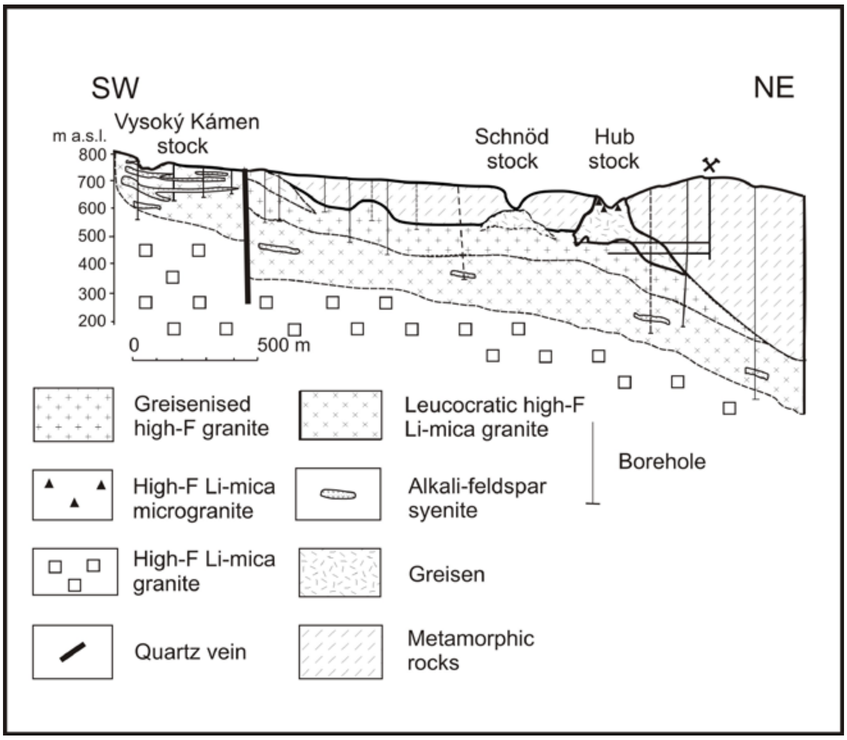

Figure 2. Geological cross section of the Horní Slavkov-Krásno ore district, modified after [19].

3. Analytical Methods

The whole rock composition of selected granitoids was analyzed in a total of 66 samples. Rock samples of 2–5 kg weight were crushed in a jaw crusher and a representative split of this material was ground to fine powder in an agate ball mill, before being pressed into XRF-tabs. Major elements were determined using a Pananalytical Axios Advanced fluorescence (XRF) (PANalytical, Almelo, The Netherlands) spectrometer at Activation Laboratories Ltd., Ancaster, ON, Canada. The content of FeO was determined by titration, H_2O^+ and H_2O^- were analyzed gravimetrically and F was analyzed using the ion selective electrode (ISE) (Krytur, Turnov, Czech Republic). Trace elements were quantified by inductively coupled plasma mass spectrometry (ICP MS) (Thermo Fisher Scientific, Waltham, MA, USA) techniques, also at Activation Laboratories Ltd., Ancaster, Canada, using a Perkin Elmer Sciex ELAN 6100 ICP mass spectrometer (PerkinElmer, Waltham, MA, USA), following standard lithium metaborate/tetraborate fusion and acid decomposition sample preparation procedures. All analyses were calibrated against international reference materials.

Approximately 230 quantitative electron probe microanalyses of monazite, xenotime, zircon, and rock-forming minerals (plagioclase, biotite) were performed in representative samples of all magmatic suites. Minerals were analyzed in polished thin sections and back-scattered electron images (BSE) were acquired to study interaction of examined accessory minerals and the internal structure of individual mineral grains. Element abundances of Al, As, Ca, Ce, Dy, Er, Eu, F, Fe, Gd, Ho, La, Lu, Mg, Mn, Na, Nd, P, Pb, Pr, S, Sc, Si, Sm, Sr, Tb, Th, Ti, Tm, U, Y, Yb, and Zr in selected accessory minerals were determined using a CAMECA SX 100 electron probe micro-analyzer (EPMA) (CAMECA, Genevilliers Cedex, France) operated in wavelength-dispersive mode. The contents of the above mentioned elements were determined using an accelerating voltage and beam current of 15 keV and 20 nA, respectively, with a beam diameter of 2–5 μm. The following standards, X-ray lines, and crystals (in parentheses) were used: AlK_α – sanidine (TAP), AsL_α – InAs (TAP), CaK_α – fluorapatite (PET); CeL_α – $CePO_4$ (PET); DyL_α – $DyPO_4$ (LIF); ErL_α – $ErPO_4$ (PET); EuL_β – $EuPO_4$ (LIF); FeK_α – almandine (LIF); GdL_β – $GdPO_4$ (LIF); HoL_β – $HoPO_4$ (LIF), LaL_α – $LaPO_4$ (PET), LuM_β – LuAG (TAP), MgK_α – Mg_2SiO_4 (TAP), MnK_α – spessartine (LIF), NdL_β – $NdPO_4$ (LIF); PK_α – fluorapatite (PET), PbM_α – vanadinite (PET); PrL_β – $PrPO_4$ (LIF), $S\,K_\alpha$ – barite (LPET), SrL_α – $SrSO_4$ (TAP), ScK_α – ScP_5O_{14} (PET); SiK_α – sanidine (TAP); SmL_β – $SmPO_4$ (LIF); TbL_α –$TbPO_4$ (LIF), ThM_α – $CaTh(PO_4)_2$ (PET), TiK_α – anatase (PET), TmL_α – $TmPO_4$ (LIF), UM_β – metallic U (PET), YL_α – YPO_4 (PET), and ZrL_α – zircon (TAP). Intra-REE overlaps were partially resolved using L_α and L_β lines. Empirically determined coincidences were applied after analysis: ThM_α on PbM_α and ThM_γ on the UM_β line. The raw data were converted into concentrations using appropriate PAP-matrix corrections [23]. The detection limits were approximately 400 ppm for Y, 180–1700 ppm for REE and 800–1000 ppm for U and Th. Mole fractions for components in monazite and xenotime were calculated according to Pyle et al. [24].

4. Results

4.1. Petrography

The medium-F biotite granite (v) is a porphyritic, fine-grained rock consisting of perthitic potassium feldspar, plagioclase ($An_{0–31}$), quartz, abundant biotite flakes (annite, ^{IV}Al 2.15–2.30 atoms per formula unit, apfu, Ti 0.37–0.55 apfu, Fe/(Fe + Mg) 0.56–0.80) and rare muscovite. Fluorapatite, zircon, monazite-(Ce), magnetite, and ilmenite are common accessory minerals.

The high-F, high-P_2O_5 topaz-bearing muscovite-biotite granite (vi) is an equigranular, medium-grained rock with abundant coarsely flaky muscovite. In addition to perthitic potassium feldspar it contains plagioclase ($An_{0–12}$), quartz, biotite (annite, ^{IV}Al 2.12–2.39 apfu, Ti 0.26–0.39 apfu, Fe/(Fe + Mg) 0.72–0.76) muscovite and topaz. Common accessory minerals are apatite, zircon, monazite, and ilmenite.

The high-F, high-P_2O_5 Li-mica granite (iii) is represented by more petrographic varieties, which could be classified as partly greisenised medium grained, equigranular granites, porphyritic, fine-grained granites and leucocratic granites that occur mainly in the Vysoký Kámen stock. The main granite variety is represented by a medium-grained, equigranular rock, consisting of quartz, albite ($An_{0–2}$), potassium feldspar, lithium mica, and topaz. Fluorapatite, zircon, Nb–Ta–Ti oxides, xenotime-(Y), and monazite-(Ce) are common accessory minerals. Cassiterite, uraninite, and coffinite occur usually as very rare accessory minerals. Porphyritic, weakly greisenised granites occur as relatively small lenses or layers in the main granite body of equigranular Li-mica granites. Their groundmass is fine-grained with phenocrysts of potassium feldspar. Granites contain quartz, albite (An_{0-5}), potassium feldspar, Li-mica and topaz. Apatite, zircon, Nb–Ta–Ti oxides, xenotime-(Y) and monazite-(Ce) are common accessories. The second sub-type of this granite, the leucocratic granite occurring in the Vysoký Kámen stock, is mostly composed of albite ($An_{0–2}$), potassium feldspar, quartz and subordinate amounts of lithium mica and topaz. Fluorapatite, Nb–Ta–Ti oxides, fluorite and rare beryl occur as accessory minerals. Quartz-free alkali-feldspar syenite (vii), composed exclusively of albite and potassium feldspar, also forms subhorizontal layers and lenses ranging from several decimetres to tens of meters in thickness in the Vysoký Kámen stock. Its contacts with leucocratic granite are typically diffuse. The alkali-feldspar syenite consists of albite ($An_{0–2}$), potassium feldspar, accessory lithium mica and topaz. Fluorapatite, triplite, Nb–Ta–Ti oxides, zircon, xenotime-(Y), monazite-(Ce), and very rare Nb-bearing wolframite are accessories. The alkali-feldspar syenite is described as feldspathite in some papers (e.g., [16,17]), but this name does not agree with the magmatic nature of this rock, which is in some places underlined by its striking magmatic layering (Figure 3).

Figure 3. Magmatic layering of alkali-feldspar syenite, Vysoký Kámen stock.

4.2. Geochemistry

The medium-F biotite granite (v) is a weakly peraluminous Ca-poor granite with aluminum saturation index (ASI) ranging from 1.1 to 1.2. In comparison with common Ca-poor granites [25] it is enriched in P (0.16–0.20 wt % P_2O_5), F (0.09–0.15 wt %), Rb (455–589 ppm), Cs (40–52 ppm), Sn(24–44 ppm), and Nb (21–23 ppm), but it is poor in Mg (0.2–0.3 wt % MgO), Ca (0.4–0.8 wt % CaO), Sr (25–64 ppm), Ba (133–207 ppm), Zr (101–170 ppm), and Y (25–31 ppm) (Table 1).

The high-F granite, high-P_2O_5 muscovite-biotite granite (vi) is a peraluminous Ca-poor S-type granite with ASI ranging from 1.2 to 1.3. In comparison with common S-type granites [25] it is enriched in P (0.14–0.27 wt % P_2O_5), F (0.17–0.31 wt %), Li (78–546 ppm), Rb (393–936 ppm), Cs (30–169 ppm), Sn (8–50 ppm), and Nb (15–32 ppm), but it is poor in Mg (0.2–0.4 wt % MgO), Ca (0.3–0.7 wt % CaO), Sr (20–91 ppm), Ba (25–394 ppm), Zr (47–111 ppm), and Y (15–34 ppm) (Table 1).

The high-F, high-P_2O_5 Li-mica granite (iii) is a highly peraluminous S-type granite with ASI ranging from 1.2 to 1.5. In comparison with typical S-type granites [25], it is enriched in P (0.26–0.31 wt % P_2O_5), F (0.04–1.00 wt %), and in incompatible elements such as Li (311–1050 ppm), Rb (830–1150 ppm), Cs (47–121 ppm), Sn (28–159 ppm), Nb (18–52 ppm), Ta (8–26 ppm) and W (3–66 ppm), but it is poor in Mg (0.1–0.4 wt % MgO), Ca (0.4–0.7 wt % CaO), Sr (10–29 ppm), Ba (6–81 ppm), Zr (24–55 ppm), and Y (5–17 ppm) (Table 1).

The leucocratic granite sub-type from the Vysoký Kámen stock is a peraluminous S-type granite with ASI ranging from 1.1 to 1.3. In comparison with high-F, high-P_2O_5, Li-mica granite it is partly enriched in P (0.33–0.69 wt % P_2O_5), Rb (670–1309 ppm), Nb (26–67 ppm), and Ta (15–33 ppm), but it is poor in Mg (0.04–0.11 wt % MgO), Ca (0.3–0.6 wt % CaO), Ba (8–25 ppm), Zr (13–26 ppm), and Y (3–7 ppm) (Table 1). Its concentrations of F are 0.14–0.16 wt %.

The alkali-feldspar syenite (vii) is a weakly peraluminous rock with ASI ranging from 1.0 to 1.1. Relative to the high-F, high-P_2O_5 Li-mica granites, the syenite is enriched in Na (4.6–6.8 wt % Na_2O), K (6.9–7.8 wt % K_2O), P (0.27–0.69 wt % P_2O_5), Rb (1760–1800 ppm), Nb (14–60 ppm), and Ta (11–44 ppm), but depleted in Si (64.0–66.5 wt % SiO_2), Mg (0.03–0.07 wt % MgO), Ca (0.3–0.5 wt % CaO), Zr (14–37 ppm), and Y (2–9 ppm) (Table 1). Its concentrations of F are 0.12–0.22 wt % (Figure 4).

The highest ΣREE content was found in the medium-F biotite granites (v) (108–168 ppm) and in the high-F granites, high-P_2O_5 muscovite-biotite granites (vi) (91–175 ppm). The high-F, high-P_2O_5 Li-mica granites (iii) and alkali-feldspar syenites (vii) exhibited lower ΣREE concentrations (3–46 ppm). For the medium-F biotite granites (v) and the high-F, high-P_2O_5 muscovite-biotite granites (vi) the higher La/Yb ratios are significant (medium-F granites 4.3–7.2, high-F, high-P_2O_5 muscovite-biotite granites 4.0–8.0), whereas the La/Yb ratios in the high-F, high-P_2O_5 granites (iii, iv) and alkali-feldspar syenites (vii) are lower (high-F, high P_2O_5 Li-mica granites 1.6–4.8, leucocratic granites 1.2–2.5, alkali-feldspar syenites 1.6–4.1). Similar differences exist also in the Eu/Eu* ratio (medium-F biotite granites 0.18–0.29, high-F, high P_2O_5 muscovite-biotite granites 0.21–0.31, high-F, high P_2O_5 Li-mica granites 0.03–0.32, leucocratic granites 0.04–0.13, alkali-feldspar syenites 0.02–0.17) (Figure 5).

Table 1. Whole-rock chemical analyses of granitic rocks of the Krudum granite body.

Sample	**Kru-126**	**1162**	**1250**	**1008**	**1192**	**1617**	**1542**	**1618**
Rock Type wt %	**Medium-F Biotite Granite**	**High-F Two-Mica Granite**	**High-F Two-Mica Granite**	**High-F Li-Mica Granite**	**High-F Li-Mica Granite**	**Leucocratic High-F Li-Mica Granite**	**Alkali-Feldspar Syenite**	**Alkali-Feldspar Syenite**
SiO_2	74.59	72.88	72.45	72.08	74.55	76.14	65.18	63.95
TiO_2	0.16	0.19	0.18	0.08	0.06	0.05	0.04	0.04
Al_2O_3	13.47	13.84	14.53	14.42	13.91	13.19	19.31	19.73
Fe_2O_3	0.15	0.35	0.32	0.12	0.05	0.10	0.37	0.32
FeO	1.43	1.08	0.96	0.89	0.93	0.04	0.04	0.29
MnO	0.06	0.03	0.03	0.06	0.06	0.01	0.02	0.02
MgO	0.21	0.43	0.32	0.22	0.14	0.05	0.07	0.07
CaO	0.38	0.64	0.46	0.71	0.49	0.31	0.39	0.27
Na_2O	3.17	3.06	3.22	3.60	3.25	4.21	4.58	5.81
K_2O	4.96	5.22	5.38	4.93	4.67	3.91	7.82	6.65
P_2O_5	0.16	0.23	0.23	0.30	0.27	0.39	0.69	0.43
H_2O^+	1.00	0.41	0.51	1.30	0.05	0.32	0.55	0.58
H_2O^-	0.31	0.64	0.46	0.00	0.39	0.12	0.10	0.14
F	0.09	0.31	0.22	0.64	0.44	0.14	0.12	0.22
O=F	0.04	0.13	0.09	0.27	0.19	0.06	0.05	0.09
Total	100.10	99.18	99.18	99.08	99.07	98.92	99.23	98.43
ASI	1.19	1.17	1.22	1.15	1.36	1.13	1.16	1.14
ppm								
Ba	144.0	296.0	488.0	47.0	55.0	23.0	22.0	31.0
Rb	588.9	543.0	580.0	883.0	1240.0	927.0	1800.0	1703.0
Sr	25.4	91.0	85.0	22.0	29.0	12.0	15.0	21.0
Y	25.2	34.2	32.8	9.0	16.7	5.7	7.0	3.4
Zr	109.6	177.0	170.0	37.0	54.0	20.0	19.0	27.0
Nb	21.3	23.5	23.3	22.0	44.0	32.1	15.1	14.4
Th	17.3	24.7	23.6	6.7	13.0	3.7	5.5	3.7
Ga	23.1	18.0	38.0	16.0	46.0	33.0	53.0	37.0
Zn	56.0	48.0	68.0	76.0	77.0	17.0	22.6	63.0
Hf	3.7	5.5	5.2	1.8	3.4	1.4	1.9	1.4
Cs	51.5	53.0	48.1	86.8	113.0	37.6	41.8	80.9
Ta	5.4	6.0	6.3	9.8	26.1	21.4	10.6	21.4
U	13.6	10.3	14.9	9.3	22.2	4.7	4.4	4.7
W	12.2	7.1	13.8	11.1	62.7	4.1	4.9	4.1
Sn	39.0	34.0	33.0	50.0	50.0	46.0	16.0	23.0
La	20.30	34.00	32.20	4.99	4.84	2.20	1.42	1.42
Ce	43.20	71.40	67.40	11.50	11.30	3.42	3.78	1.69
Pr	5.08	8.20	7.90	1.38	1.30	0.41	0.48	0.21
Nd	19.40	31.10	29.60	5.05	5.43	2.12	1.82	1.15
Sm	3.95	7.29	6.75	1.41	1.81	0.67	0.75	0.38
Eu	0.22	0.72	0.68	0.06	0.10	0.01	0.02	0.01
Gd	3.54	6.72	6.48	1.24	1.93	0.61	0.76	0.34
Tb	0.71	1.20	1.13	0.28	0.46	0.14	0.21	0.08
Dy	4.18	6.51	6.04	1.71	1.67	0.94	1.18	0.52
Ho	0.88	1.15	1.06	0.29	0.28	0.16	0.19	0.09
Er	2.61	3.30	3.08	0.84	1.67	0.47	0.48	0.27
Tm	0.43	0.47	0.47	0.14	0.28	0.09	0.09	0.06
Yb	3.22	2.88	2.72	1.04	2.02	0.59	0.62	0.37
Lu	0.41	0.39	0.37	0.12	0.28	0.08	0.08	0.05
ΣREE	108.13	175.34	165.87	30.06	34.92	11.90	11.88	6.63
La_N/Yb_N	4.25	7.96	7.98	3.23	1.62	2.52	1.55	2.59
Eu/Eu*	0.18	0.31	0.31	0.14	0.17	0.04	0.06	0.09

Eu/Eu*—$Eu_N/\sqrt{[(Sm_N) \times (Gd_N)]}$.

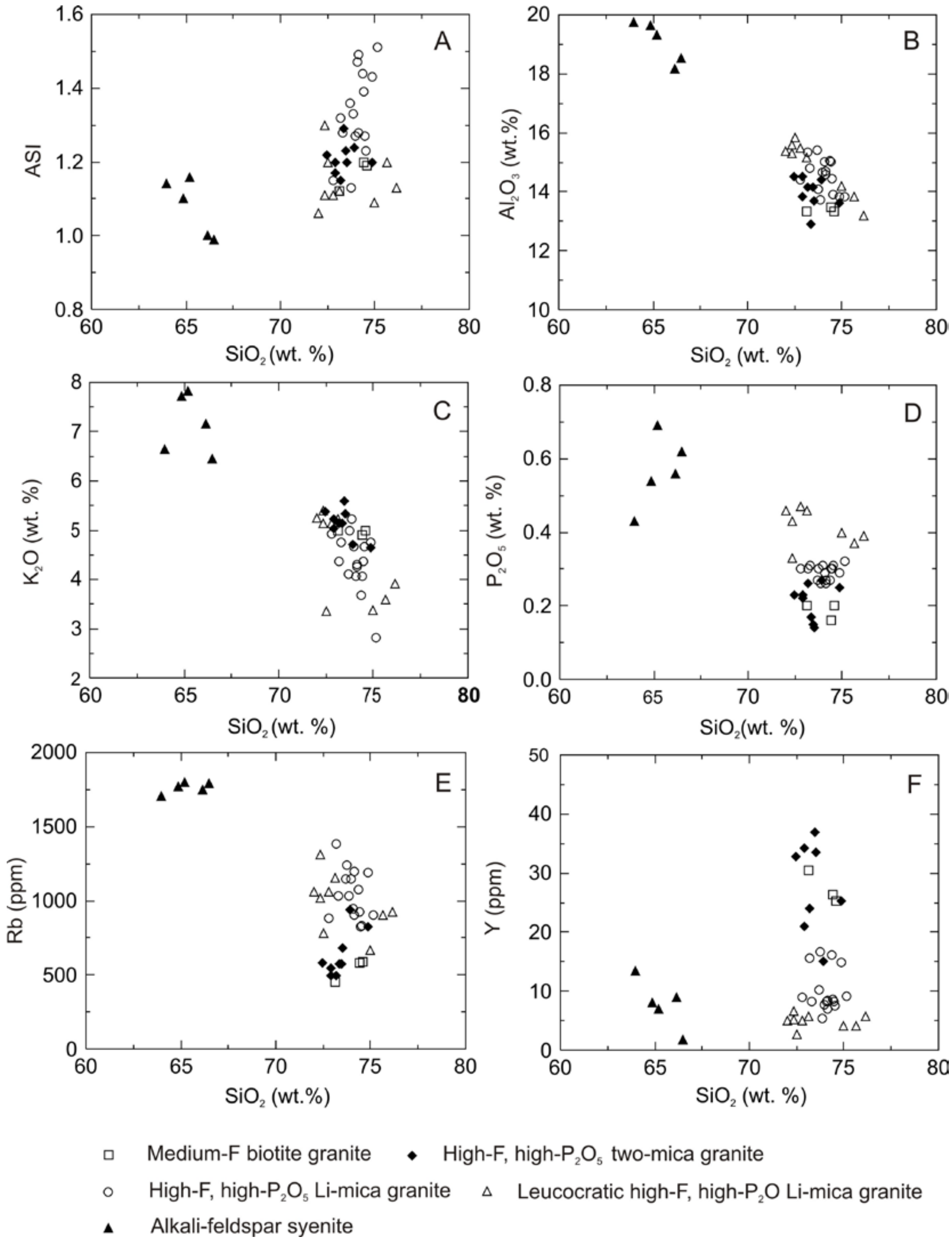

Figure 4. (**A**) Binary plot of ASI vs. SiO_2 for granitic rocks of the Krudum granite body, (**B**) Binary plot of Al_2O_3 vs. SiO_2 for granitic rocks of the Krudum granite body, (**C**) Binary plot of K_2O vs. SiO_2 for granitic rocks of the Krudum granite body, (**D**) Binary plot of P_2O_5 vs. SiO_2 for granitic rocks of the Krudum granite body (**E**) Binary plot of Rb vs. SiO_2 for granitic rocks of the Krudum granite body, (**F**) Binary plot of Y vs. SiO_2 for granitic rocks of the Krudum granite body.

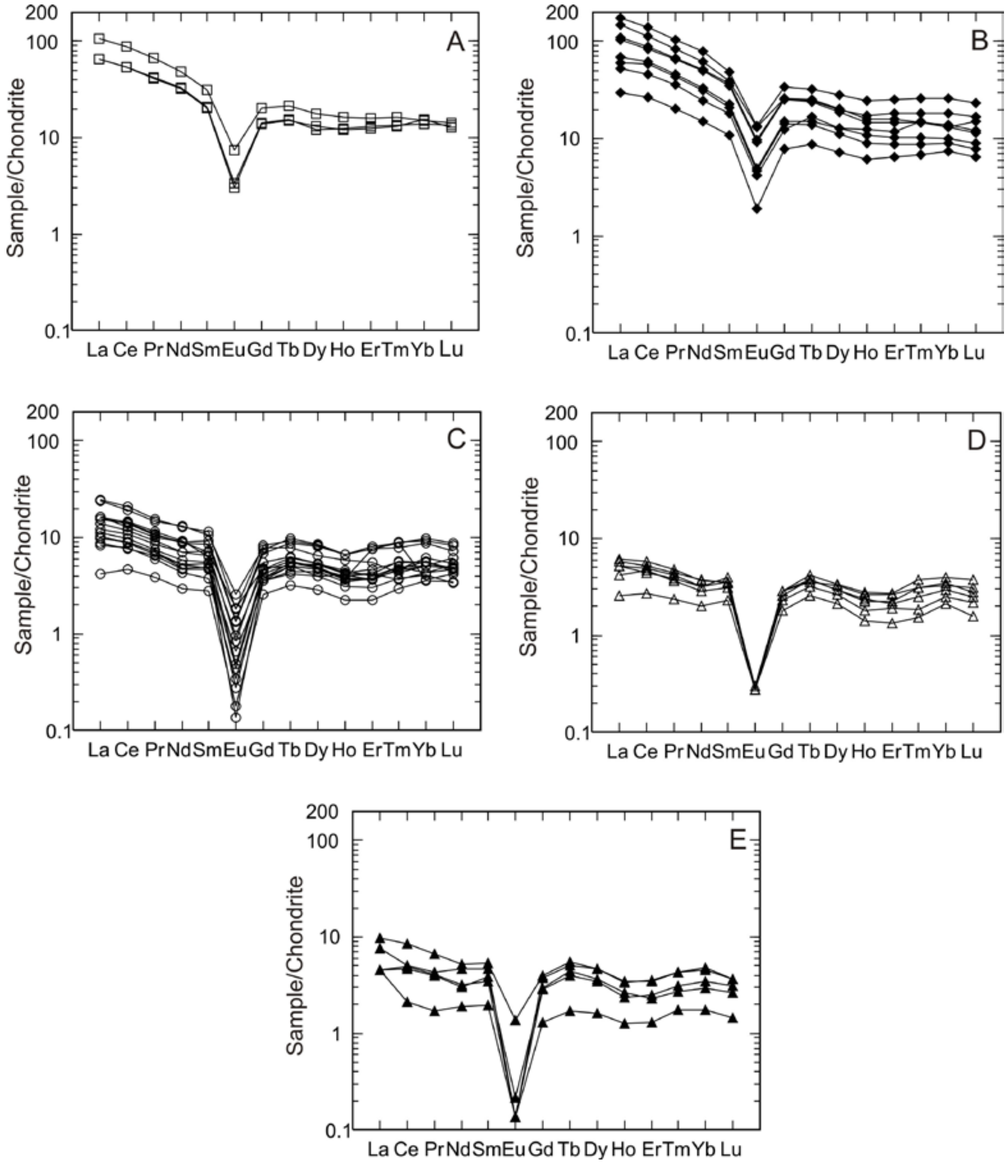

Figure 5. Chondrite-normalized rare earth element (REE) patterns for granitic rocks of the Krudum granite body. (**A**) Chondrite-normalized rare earth element (REE) patterns for medium-F biotite granite, (**B**) Chondrite-normalized rare earth element (REE) patterns for high-F, high-P_2O_5 two-mica granite, (**C**) Chondrite-normalized rare earth element (REE) patterns for high-F, high-P_2O_5 Li-mica granite, (**D**) Chondrite-normalized rare earth element (REE) patterns for leucocratic high-F, high-P_2O_5 Li-mica granite, (**E**) Chondrite normalized rare earth element (REE) patterns for alkali–feldspar syenite. Normalizing values are from [26].

4.3. REE and Y Mineralogy

4.3.1. Accessory Minerals Textures

In the granite suites of the KGB rare earth element- (REE) and Y-bearing accessory minerals are represented by monazite, xenotime, and zircon. Monazite and zircon occur in all magmatic suites, whereas xenotime was found only in the high-F, high-P_2O_5 Li-mica granites (iii) and in the alkali-feldspar syenites (vii). Monazite, together with zircon and fertile apatite is usually enclosed in biotite and lithium mica flakes. Monazite occurs as small subhedral to anhedral grains (10–30 µm), often grows together with zircon in complex aggregates together with coffinite and xenotime (Figure 6).

Monazite grains are not zoned, but zircon may have oscillatory zoning (Figure 7). Cores of possible inherited zircon grains were overgrown by younger zircon and xenotime (Figure 7D). The xenotime occurs as grains along the zircon rims (Figures 6 and 7B).

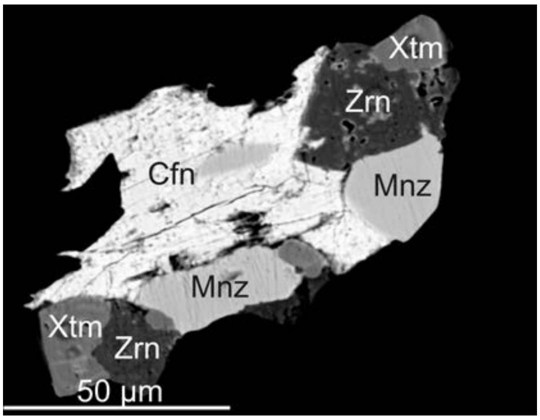

Figure 6. High-contrast back-scattered electron (BSE) image of complex intergrowths of coffinite (Cfn), zircon (Zrn), monazite (Mnz), and xenotime (Xtm) from high-F, high-P_2O_5 Li-mica granite, Hub stock.

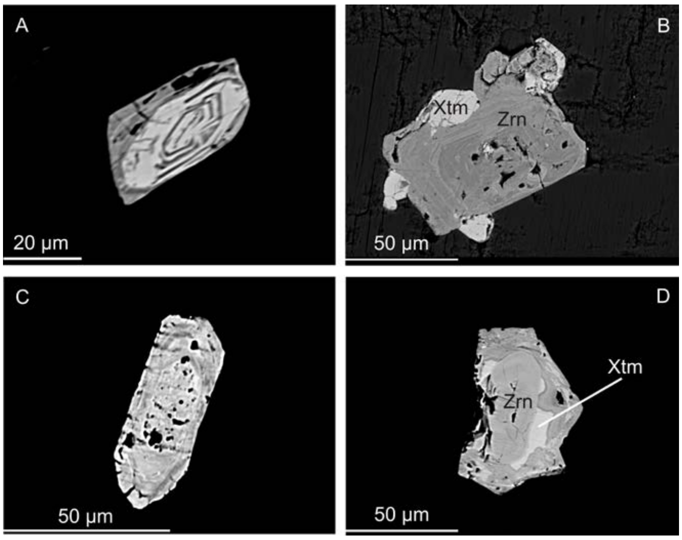

Figure 7. High-contrast BSE images of zircon (Zrn) and xenotime (Xtm) from granites of the Krudum granite body. (**A**) Oscillatory zoning of zircon from the medium-F biotite granite, (**B**) Intergrowth of xenotime with zircon from the high-F, high-P_2O_5 Li-mica granite, (**C**) Oscillatory zoning of altered zircon in the high-F, high-P_2O_5 Li mica granite, (**D**) Inherited zircon grains overgrown by younger zircon and xenotime from the high-F, high-P_2O_5 Li-mica granite.

4.3.2. Monazite Composition

Monazite strongly favors LREE entrapment with the sum of LREE (La + Ce + Pr + Nd + Sm) ranging between 0.21 and 0.94 apfu (atoms per formula unit) (Table 2). Cerium is, in all cases, the most abundant REE, varying between 7.95 wt % Ce_2O_3 and 32.57 wt % Ce_2O_3 (0.12–0.48 apfu Ce). The second most abundant REE is La (2.06–15.44 wt % La_2O_3; 0.03–0.23 apfu La), followed by Nd (2.05–12.04 wt % Nd_2O_3; 0.03–0.17 apfu Nd), Pr (1.80–3.49 wt % Pr_2O_3; 0.03–0.05 apfu Pr) and Sm (1.44–3.48 wt % Sm_2O_3; 0.02–0.05 apfu Sm). Thus, all analyzed monazite grains should be termed monazite-(Ce). However, the ranges in chondrite ratios between individual LREE vary considerably: the $(La/Nd)_{CN}$ ratio between 0.46 and 3.39, the $(La/Sm)_{CN}$ ratio between 0.49 and 6.27.

Table 2. Representative EPMA of monazite.

Sample	KRU-34	KRU-35	1162-2	1162-13	1008-33	1371-3	1617-26
Variety wt %	Medium-F Granite	Medium-F Granite	High-F Two-Mica Granite	High-F Two-Mica Granite	High-F Li-Mica Granite	High-F Li-Mica Granite	Alkali-Feldspar Syenite
P_2O_5	29.27	29.09	29.22	28.12	28.70	28.67	30.18
SiO_2	0.62	0.75	0.58	0.55	1.15	0.63	0.27
ThO_2	8.23	10.33	5.81	2.71	10.08	24.53	32.82
UO_2	0.93	0.88	1.23	0.19	0.31	2.13	4.54
Y_2O_3	2.13	2.53	2.91	0.38	3.38	2.12	1.49
La_2O_3	11.68	11.36	11.51	15.44	10.47	4.80	3.84
Ce_2O_3	26.29	24.73	26.17	32.57	25.22	15.42	9.19
Pr_2O_3	2.80	2.77	3.03	3.49	2.95	1.98	1.01
Nd_2O_3	10.02	9.48	11.36	12.04	10.60	6.79	3.39
Sm_2O_3	1.79	1.81	2.54	1.88	2.25	2.84	0.97
Gd_2O_3	1.20	1.12	1.95	0.72	1.83	1.75	0.80
Dy_2O_3	0.80	0.80	1.02	0.11	1.14	1.02	0.59
Er_2O_3	0.17	0.17	0.21	0.03	0.23	0.14	0.11
CaO	1.30	1.75	1.53	0.32	1.29	5.18	8.04
PbO	0.17	0.17	0.16	0.04	0.14	0.42	0.62
As_2O_5	0.03	0.06	0.05	0.06	0.04	b.d.l.	0.08
F	b.d.l.	b.d.l.	b.d.l.	0.01	0.56	b.d.l.	0.40
O=F	0.00	0.00	0.00	0.00	0.14	0.00	0.10
Total	97.43	97.80	99.28	98.66	100.20	98.42	98.24
apfu, O=4							
P	0.986	0.977	0.973	0.960	0.955	0.969	1.000
Si	0.025	0.030	0.023	0.022	0.045	0.025	0.011
Th	0.075	0.093	0.052	0.025	0.090	0.223	0.292
U	0.008	0.008	0.011	0.002	0.003	0.019	0.040
Y	0.045	0.053	0.061	0.008	0.071	0.045	0.031
La	0.171	0.166	0.167	0.230	0.152	0.071	0.055
Ce	0.383	0.359	0.376	0.481	0.363	0.225	0.131
Pr	0.041	0.040	0.043	0.051	0.042	0.029	0.014
Nd	0.142	0.134	0.159	0.173	0.149	0.097	0.047
Sm	0.025	0.025	0.034	0.026	0.030	0.039	0.013
Gd	0.016	0.015	0.025	0.010	0.024	0.023	0.010
Dy	0.010	0.010	0.013	0.001	0.014	0.013	0.007
Er	0.002	0.002	0.003	0.000	0.003	0.002	0.001
Ca	0.055	0.074	0.064	0.014	0.054	0.222	0.337
Pb	0.002	0.002	0.002	0.000	0.001	0.005	0.007
As	0.001	0.001	0.001	0.001	0.001	0.000	0.002
F	0.000	0.000	0.000	0.003	0.139	0.000	0.087
$LREEPO_4$	0.7758	0.7312	0.7633	0.9397	0.7308	0.4333	0.2541
$HREEPO_4$	0.0295	0.0282	0.0420	0.0111	0.0424	0.0390	0.0185
$CaTh(PO_4)_2$	0.1158	0.1548	0.1311	0.0281	0.1118	0.4559	0.6934
$ThSiO_4$	0.0316	0.0303	0.0010	0.0131	0.0414	0.0257	0.0021
YPO_4	0.0474	0.0554	0.0625	0.0080	0.0735	0.0462	0.0319

b.d.l., below detection limit.

The content of Y in analyzed monazite ranges from 0.07 to 4.26 wt % Y_2O_3 (0.00–0.09 apfu Y). The highest concentrations of Y were found in monazite from the alkali-feldspar syenites (up to 4.26 wt % Y_2O_3; 0.09 apfu Y). The concentrations of ΣHREE (Gd + Dy + Er) in analyzed monazite grains range from 0.00 to 0.05 apfu. The concentrations of Th vary between 2.71 and 35.42 wt % ThO_2 (0.03–0.33 apfu Th). The high-Th monazite with 32.8–35.4 wt % ThO_2 (0.29–0.33 apfu Th) was found in some monazite grains from the alkali-feldspar syenites. The concentrations of U vary between 0.19 and 4.54 wt % UO_2 (0.00–0.04 apfu U). Monazite from the high-F, high-P_2O_5 Li-mica granites and alkali-feldspar syenites is sometimes fluorized (up to 0.78 wt % F; 0.23 apfu F). These partly altered monazite grains contain also low concentrations of As (up to 0.08 wt % As_2O_5; 0.002 apfu As) and S (up to 0.06 wt % SO_3; 0.002 apfu S).

Two main coupled substitution mechanisms have been proposed for monazite [2,27,28], namely the cheralite and huttonite substitutions. The analyzed monazite grains from all of the KGB magmatic suites plot between the cheralite and huttonite substitution vectors in the (Th + U + Si) vs. the (P + Y + REE) diagram. The huttonite substitution is characteristic for monazite from the low-F biotite granites (Figure 8).

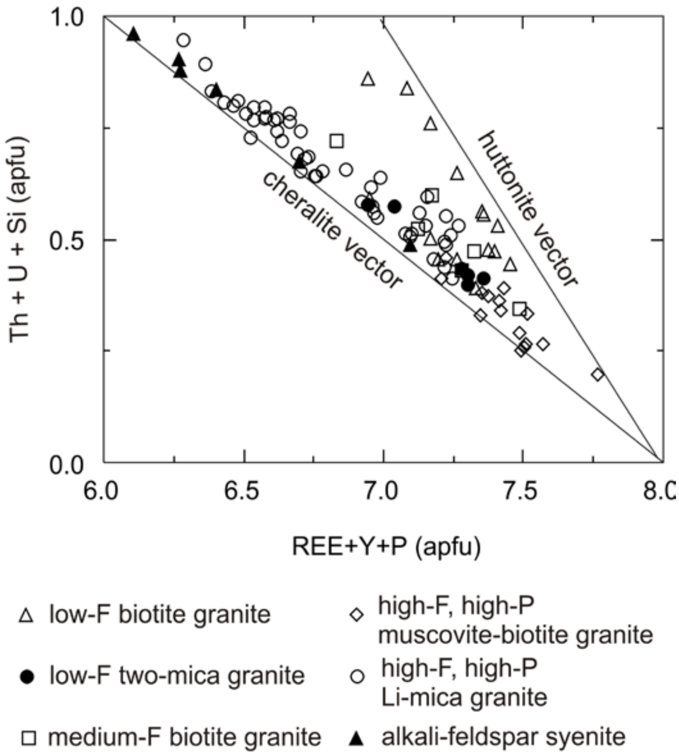

Figure 8. Monazite composition vectors of monazite from the Krudum granite body.

The highest fractions of the cheralite component were found in monazite from the alkali-feldspar syenites (vii) (up to 69.3 mol %). Similarly, the concentration of the xenotime (YPO_4) component is relatively high in monazite from the high-F, high-P_2O_5 granites (iii, iv) (up to 9.1 mol %) and from the alkali-feldspar syenites (vii) (up to 9.4 mol %).

4.3.3. Xenotime Composition

The proportion of YPO_4, the main component in xenotime, ranges from 70.66 to 83.75 mol % (Table 3). Some microprobe analyses from the high-F, high-P_2O_5 Li-mica granites reveal low totals, suggesting probably hydration of xenotime during its postmagmatic alteration. In slightly greisenised high-F, high-P_2O_5 Li-mica granites from the Hub stock of the F content reaches up to 1.12 wt %. Analyzed xenotime grains are commonly enriched in HREE (9.3–19.5 wt %$HREE_2O_3$), U and Th. The concentrations of Dy and Yb range from 3.05 to 7.67 wt % Dy_2O_3 (0.04–0.08 apfu Dy) and 2.24 to 8.04 wt % Yb_2O_3 (0.03–0.09 apfu Yb); the concentrations of U and Th range from 0.45 to 5.55 wt %UO_2 (0.00–0.04 apfu U) and 0.04-1.73 wt % ThO_2 (0.00–0.01 apfu Th). Two charge balancing coupled substitutions involving Si (thorite-coffinite exchange, 0.0–4.5 mol % thorite component) and/or Ca (cheralite exchange, 1.2–19.8 mol % cheralite component) for the replacement of Y and REE by U and Th are observed in xenotime. Both substitution mechanisms are found in the high-F, high-P_2O_5 Li-mica granites (Figure 9). In some cases, the xenotime grains are enriched in Sc (up to 2.03 wt % Sc_2O_3; 0.25 apfu Sc), Zr (up to 1.62 wt % ZrO_2; 0.03 apfu Zr) and Bi (up to 0.07 wt % Bi_2O_3; 0.002 apfu Bi).

The Sc and Bi contents show a lack of correlation with other cations in the octahedral position. The Zr content shows a negative correlation with Y content.

Table 3. Representative EPMA of xenotime.

Sample	1007-4	1007-11	1007-19	997-9	1542-18	1542-20
Variety wt %	High-F Li-Mica Granite	High-F Li-Mica Granite	High-F Li-Mica Granite	Alkali-Feldspar Syenite	Alkali-Feldspar Syenite	Alkali-Feldspar Syenite
P_2O_5	34.50	36.31	33.87	31.99	32.75	33.00
SiO_2	0.96	b.d.l.	0.85	0.23	0.97	0.93
ThO_2	0.87	0.04	0.72	0.53	1.50	1.29
UO_2	4.43	0.93	4.56	2.49	3.06	2.97
Y_2O_3	38.83	48.50	38.23	39.59	40.18	40.19
La_2O_3	b.d.l.	0.03	0.01	b.d.l.	b.d.l.	0.01
Ce_2O_3	b.d.l.	b.d.l.	0.03	0.04	0.11	0.14
Pr_2O_3	b.d.l.	0.02	0.07	0.10	0.08	0.05
Nd_2O_3	0.32	0.08	0.42	0.26	0.38	0.44
Sm_2O_3	0.87	0.11	0.79	0.84	0.67	0.68
Gd_2O_3	2.56	0.61	2.38	2.72	2.29	2.21
Dy_2O_3	7.59	3.79	7.35	6.69	6.16	6.19
Ho_2O_3	0.98	0.69	1.06	b.d.l.	b.d.l.	b.d.l.
Er_2O_3	3.23	2.48	3.42	3.15	3.45	3.43
Yb_2O_3	4.23	3.81	3.96	4.50	2.31	2.36
Lu_2O_3	0.81	0.56	0.91	0.02	b.d.l.	b.d.l.
CaO	0.42	0.89	0.51	0.49	0.19	0.16
PbO	0.18	0.02	0.10	0.43	0.51	0.51
F	0.09	1.12	0.10	0.05	0.10	0.02
O=F	0.04	0.47	0.04	0.02	0.04	0.01
Total	100.83	99.52	99.30	94.10	94.67	94.57
apfu, O=4						
P	0.985	1.001	0.984	0.973	0.974	0.978
Si	0.032	0.000	0.029	0.008	0.034	0.033
Th	0.007	0.000	0.006	0.004	0.012	0.010
U	0.033	0.007	0.035	0.020	0.024	0.023
Y	0.696	0.840	0.697	0.756	0.750	0.748
La	0.000	0.000	0.000	0.000	0.000	0.000
Ce	0.000	0.000	0.000	0.001	0.001	0.002
Pr	0.000	0.000	0.001	0.001	0.001	0.001
Nd	0.004	0.001	0.005	0.003	0.005	0.005
Sm	0.010	0.001	0.009	0.010	0.008	0.008
Gd	0.029	0.007	0.027	0.032	0.027	0.026
Dy	0.082	0.040	0.081	.0.077	0.070	0.070
Ho	0.010	0.007	0.012	0.000	0.000	0.000
Er	0.034	0.025	0.037	0.036	0.038	0.038
Yb	0.043	0.038	0.041	0.049	0.025	0.025
Lu	0.008	0.006	0.009	0.000	0.000	0.000
Ca	0.015	0.031	0.019	0.019	0.007	0.006
Pb	0.002	0.000	0.001	0.004	0.005	0.005
F	0.019	0.231	0.022	0.011	0.022	0.004
$LREEPO_4$	0.0144	0.0020	0.0153	0.0148	0.0154	0.0165
$HREEPO_4$	0.2117	0.1226	0.2112	0.1917	0.1644	0.1644
$CaTh(PO_4)_2$	0.0308	0.0616	0.0388	0.0375	0.0144	0.0124
$ThSiO_4$	0.0270	0.0000	0.0230	0.0090	0.0340	0.0320
YPO_4	0.7153	0.8375	0.7112	0.7470	0.7708	0.7735

b.d.l., below detection limit.

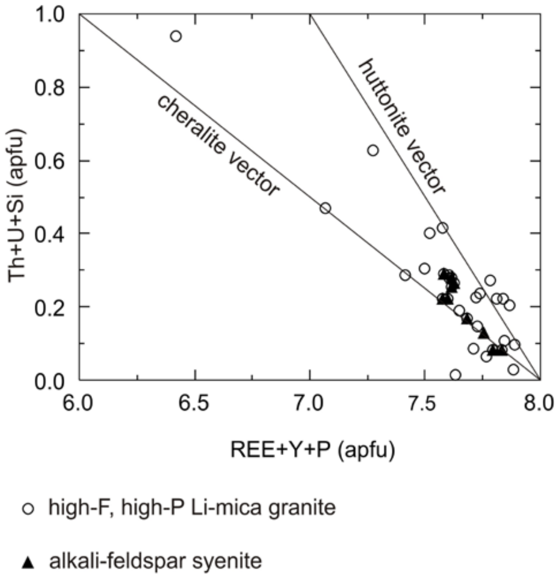

Figure 9. Xenotime composition vectors of xenotime from the Krudum granite body.

4.3.4. Zircon Composition

Analyzed zircon grains contain moderate Hf concentrations (1.0–4.7 wt % HfO_2; 0.010–0.047 apfu Hf) (Table 4, Figure 10). The proportion of the hafnium end member indicated by atomic ratio Hf/(Zr + Hf) varies from 0.01 to 0.05. The highest concentrations of HfO_2 were found in zircon from the high-F, high-P_2O_5 Li-mica granites (1.2–4.7 wt % HfO_2). In the zircon from the medium-F biotite granites (v) and the high-F, high-P_2O_5 muscovite-biotite granites (vi) HfO_2 concentrations are distinctly lower (1.0–2.5 wt %).

Table 4. Representative EPMA of zircon.

Sample	23-44	23-45	1162-5	1250-27	1007-2	1283-21	997-1	1542-2
Variety wt %	Medium-F Granite	Medium-F Granite	High-F Two-Mica Granite	High-F Two-Mica Granite	High-F Li-Mica Granite	High-F Li-Mica Granite	Alkali-Feldspar Syenite	Alkali-Feldspar Syenite
SiO_2	31.60	32.16	31.85	32.30	31.49	26.49	32.32	24.22
Al_2O_3	b.d.l.	b.d.l.	b.d.l.	b.d.l.	b.d.l.	0.11	0.01	0.85
ZrO_2	64.19	65.40	63.05	66.00	61.73	49.81	65.32	54.02
HfO_2	1.43	1.03	2.52	1.36	3.60	1.83	1.33	2.67
CaO	0.01	0.03	0.05	b.d.l.	0.03	0.40	0.04	1.54
FeO	b.d.l.	b.d.l.	0.05	0.02	0.16	0.01	0.02	1.61
MnO	0.02	b.d.l.	0.02	b.d.l.	0.04	0.03	0.02	b.d.l.
MgO	b.d.l.	0.01	0.01	0.02	b.d.l.	b.d.l.	0.01	0.04
P_2O_5	0.50	0.05	0.59	0.02	0.79	5.46	0.38	4.58
Sc_2O_3	0.11	b.d.l.	0.35	b.d.l.	0.31	0.42	0.09	0.50
As_2O_5	b.d.l.	b.d.l.	0.01	0.05	0.10	0.05	0.04	0.30
Bi_2O_3	0.09	0.08	0.05	0.10	0.07	0.12	0.09	0.10
Y_2O_3	0.48	0.23	0.26	b.d.l.	0.38	5.47	0.20	0.17
La_2O_3	b.d.l.	b.d.l.	b.d.l.	b.d.l.	0.02	0.02	0.02	b.d.l.
Ce_2O_3	b.d.l.	b.d.l.	0.02	b.d.l.	b.d.l.	0.36	0.01	0.09
Pr_2O_3	0.03	b.d.l.	b.d.l.	0.03	b.d.l.	0.02	0.02	0.06
Nd_2O_3	b.d.l.	0.10	b.d.l.	b.d.l.	0.04	0.02	0.08	0.06
Sm_2O_3	0.01	0.01	b.d.l.	0.01	b.d.l.	0.11	b.d.l.	0.05
Gd_2O_3	b.d.l.	0.01	0.01	b.d.l.	b.d.l.	0.35	0.02	0.02
Dy_2O_3	0.03	0.05	0.01	b.d.l.	b.d.l.	0.81	0.02	b.d.l.
Er_2O_3	0.12	0.07	0.02	0.06	0.10	0.50	0.06	0.05
Yb_2O_3	0.21	0.06	0.18	0.03	0.29	0.78	0.05	0.15
UO_2	0.50	0.09	0.65	0.04	0.52	3.09	0.11	2.06
ThO_2	0.01	0.04	0.02	0.02	0.01	0.92	b.d.l.	0.25

b.d.l., below detection limit.

Table 4. *Cont.*

Sample	23-44	23-45	1162-5	1250-27	1007-2	1283-21	997-1	1542-2
Variety wt %	Medium-F Granite	Medium-F Granite	High-F Two-Mica Granite	High-F Two-Mica Granite	High-F Li-Mica Granite	High-F Li-Mica Granite	Alkali-Feldspar Syenite	Alkali-Feldspar Syenite
PbO	0.02	b.d.l.	0.03	b.d.l.	0.04	0.87	0.01	0.03
F	b.d.l.	b.d.l.	0.03	b.d.l.	b.d.l.	0.28	0.01	0.65
O=F	0.00	0.00	0.01	0.00	0.00	0.12	0.00	0.27
Total	99.36	99.42	99.77	100.06	99.68	98.33	100.28	94.07
apfu, O=4								
Si	0.982	0.995	0.987	0.994	0.981	0.859	0.990	0.810
P	0.013	0.001	0.015	0.001	0.021	0.150	0.010	0.130
Al	0.000	0.000	0.000	0.000	0.000	0.004	0.000	0.033
ΣT-site	0.995	0.996	1.002	0.995	1.002	1.013	1.000	0.973
Zr	0.973	0.987	0.952	0.990	0.938	0.788	0.976	0.881
Hf	0.013	0.009	0.022	0.012	0.032	0.017	0.012	0.025
Ca	0.000	0.001	0.002	0.000	0.001	0.014	0.001	0.055
Fe	0.000	0.000	0.001	0.001	0.004	0.000	0.001	0.045
Mn	0.001	0.000	0.001	0.000	0.001	0.001	0.001	0.000
Mg	0.000	0.000	0.000	0.001	0.000	0.000	0.000	0.002
Sc	0.003	0.000	0.009	0.000	0.008	0.012	0.002	0.015
As	0.000	0.000	0.000	0.001	0.002	0.001	0.001	0.005
Bi	0.000	0.000	0.000	0.001	0.000	0.001	0.000	0.001
Y	0.008	0.004	0.004	0.000	0.006	0.094	0.003	0.003
La	0.000	0.000	0.000	0.000	0.000	0.000	0.000	0.000
Ce	0.000	0.000	0.000	0.000	0.000	0.004	0.000	0.001
Pr	0.000	0.000	0.000	0.000	0.000	0.000	0.000	0.001
Nd	0.000	0.001	0.000	0.000	0.000	0.001	0.001	0.001
Sm	0.000	0.000	0.000	0.000	0.000	0.001	0.000	0.001
Gd	0.000	0.000	0.000	0.000	0.000	0.004	0.000	0.000
Dy	0.000	0.000	0.000	0.000	0.000	0.008	0.000	0.000
Er	0.001	0.001	0.000	0.001	0.001	0.005	0.001	0.001
Yb	0.002	0.001	0.002	0.000	0.003	0.008	0.000	0.002
U	0.003	0.001	0.004	0.000	0.004	0.022	0.001	0.015
Th	0.000	0.000	0.000	0.000	0.000	0.007	0.000	0.002
Pb	0.000	0.000	0.000	0.000	0.000	0.008	0.000	0.000
ΣA site	1.004	1.005	0.997	1.007	1.000	0.996	1.000	1.056
F	0.000	0.000	0.006	0.000	0.000	0.057	0.002	0.137

b.d.l., below detection limit.

Analyzed zircon grains from the high-F, high-P_2O_5 Li mica granites (iii) and from alkali-feldspar syenites (vii) are enriched in P (up to 8.29 wt %P_2O_5; 0.24 apfu P), Al (0.02–2.0 wt % Al_2O_3; 0.00–0.08 apfu Al; berlinite substitution), Ca (up to 3.9 wt % CaO; 0.14 apfu Ca; brabantite substitution), Y (up to 5.5 wt % Y_2O_3; 0.10 apfu Y; xenotime substitution) and Sc (up to 1.17 wt % Sc_2O_3; 0.03 apfu Sc; pretulite substitution) (Figure 11). Zircon grains from the high-F, high-P_2O_5 Li-mica granites (iii) and alkali-feldspar syenites (vii) are in some cases metamictized, hydrated and fluorized. Partly hydrothermally altered zircon grains from high-F, high-P_2O_5 Li-mica granites (iii) are also enriched in Bi (up to 5.16 wt % Bi_2O_3; 0.03 apfu Bi; ximengite substitution). Zircon grains from the alkali-feldspar syenites have a higher enrichment in P, which is not associated with a simultaneous enrichment in Y + REE (Figure 11). The uranium and thorium are ubiquitous components in all analyzed zircon grains, especially in the altered zircon from high-F, high-P_2O_5 Li-mica granites. High concentrations of U, up to 3.1 wt % UO_2 (0.02 apfu U), were found in zircon from these granites. The concentrations of Th in altered zircons from high-F, high-P_2O_5 Li-mica granites are between 0.2 and 1.7 wt % ThO_2 (0.00–0.01 apfu Th). Concentrations of U and Th in zircon from the medium-F biotite granites and from the high-F, high-P_2O_5 muscovite-biotite granites are lower (0.04–0.65 wt % UO_2; 0.01–0.21 wt % ThO_2).

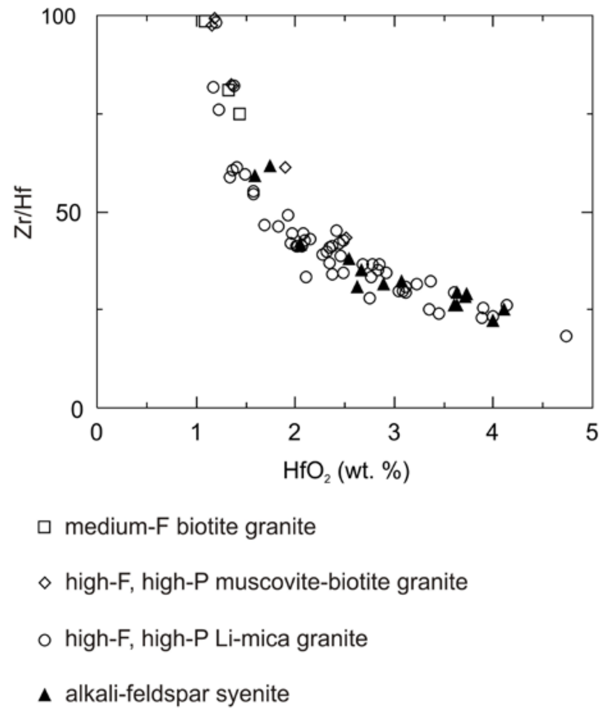

Figure 10. Chemical composition of zircon from granites of the Krudum granite body.

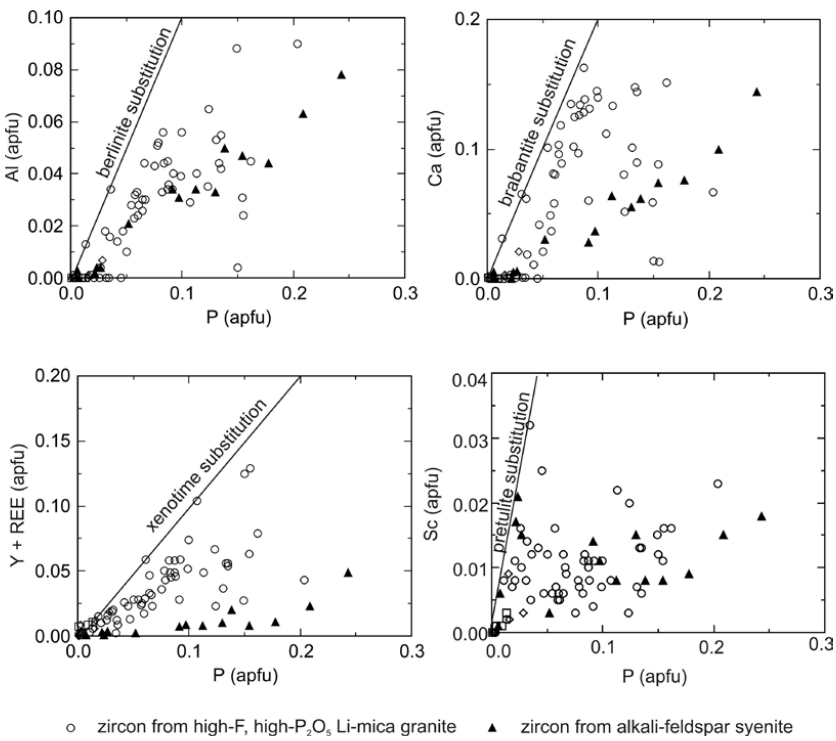

Figure 11. Chemical compositions of zircon from the high-F, high-P_2O_5 Li-mica granites and alkali-feldspar syenites. (**A**) Distribution Al vs. P. The arrow represent vector of ideal berlinite type (P:Al = 1:1) substitution, (**B**) Distribution Ca vs. P. The arrow represent vector of ideal brabantite-type (P:Ca = 2:1) substitution, (**C**) Distribution of Y and REE vs. P. The arrow represent vector of ideal xenotime-type (P:(Y + REE) = 1:1) substitution, (**D**) Distribution Sc vs. P. The arrow represent vector of ideal pretulite-type (P:Sc = 1:1) substitution.

5. Discussion

5.1. Substitution in Monazite

Two main coupled substitutions mechanisms have been proposed for monazite, the cheralite substitution $(Th,U)^{4+} + Ca^{2+} = 2REE^{3+}$ and the huttonite substitution $(Th,U)^{4+} + Si^{4+} = REE^{3+} + P^{5+}$ [27–31]. The cheralite substitution is dominant in the analyzed monazite from all the analyzed suites of the KGB. The predominance of the cheralite substitution over the huttonite substitution was also found in highly fractionated high-F, Li-mica granites from other parts of the Krušné Hory/Erzgebirge batholith and the Fichtelgebirge granites in NE Bavaria, Germany [3,9,27]. High contents of the cheralite component (>20–30 mol %) were also found in highly fractionated S-type granites from the West Carpathian belt [2] and in similar S-type granites from the Belvís de Monroy pluton in the Iberian Variscan belt [7]. The high-Th monazite was found also in the high-F, high-P_2O_5 Li-mica granites from the German part of the Western Erzgebirge pluton (up to 51.7 wt % ThO_2) [27]. Some monazite grains from similar high-F granites described in the Fichtelgebirge pluton [3] could be designed also as high-Th monazite.

5.2. Substitution in Xenotime

Like for monazite, two main mechanisms exist for the replacement of Y by REE, U and Th in xenotime: charge balancing coupled substitutions involving Si and Ca (thorite-coffinite-type and cheralite-type substitutions respectively) [2,5,31,32]. In the analyzed xenotime from high-F, high P_2O_5 granites (iii, iv) both substitutions mechanisms exist. Both mechanisms were also found in the S-type, high-F, Li-mica granites from the German part of Krušné Hory/Erzgebirge area [32]. However, according to Pérez-Soba et al. [7], unlike zircon, xenotime from highly fractionated peraluminous granites from the Belvís de Monroy pluton in the Iberian Variscan belt showed predominance of one substitution, the cheralite substitution, over the thorite-coffinite substitution.

5.3. Substitution in zircon

The highest concentrations of P in zircon are accompanied by a simultaneous enrichment in Al. This correlation can be explained by the occurrence of berlinite-type substitution $P^{5+} + Al^{3+} = 2Si^{4+}$. This substitution is significant for zircon from other high-F, high-P_2O_5 Li-mica granites in the Western Erzgebirge pluton (Podlesí granite stock [33]). A combination of berlinite, xenotime $(REE + Y)^{+3} + P^{+5} = Zr^{4+} + Si^{4+}$), pretulite ($Sc^{3+} + P^{5+} = Zr^{4+} + Si^{4+}$) and brabantite ($Ca^{2+}(U,Th)^{4+} + 2\,P^{5+} = 2Zr^{4+} + 2Si^{4+}$) types is also significant in zircon grains from these granites [33]. Anomalous enrichment of P from alkali-feldspar syenite is similar to that was found in zircon from the dyke granites in the Podlesí granite stock [33].

Enrichment of non-formula elements such as P, Al, Ca, Y and REE in P-rich zircon was found also in some other high-P peraluminous granites worldwide [7,34–36]. The entry of Y + HREE and P into the zircon structure is usually explained via xenotime substitution, whereas zircon and xenotime are isostructural [37–39]. The apparent surplus on the A-site could be explained by the entrance of substantial amounts of interstitial cations (e.g., Fe, Ca, Al, As, Bi, Sc) [40,41]. Sc enrichment in zircon is usually explained via the pretulite ($ScPO_4$) exchange [42]. However, rational evaluation of non-formula elements enrichment in zircon is always matter of discussion. The most extended explanation is usually coupled with its metamictization and later postmagmatic alteration [43–45]. Higher concentrations of P, Y and REE occur in metamictized zircon grains from the high-F, high-P_2O_5 Li-mica granites (Figures 6 and 7C). Description of postmagmatic zircon alterations from these granites was presented in detail by René [46]. On the other hand, the berlinite substitution found in zircon grains from the Podlesí granite stock and Belvís de Monroy pluton (Iberian Variscan belt) is believed to by primary magmatic [7,33]. Similarly, the highest concentration of P (8.29 wt % P_2O_5; 0.24 apfu P) was found in primary magmatic zircon grain from the examined alkali feldspar syenite.

Moderate to strong deviation of altered zircon from stoichiometry was also found in other occurrences of high-F, Li-mica granites in the Krušné Hory/Erzgebirge area (e.g., Cínovec, Podlesí, Altenberg, Seifen [33,36,47,48] as well as in altered zircon worldwide [49–54].

6. Conclusions

(a) The Krudum granite body has a sequence of highly fractionated granitic rocks from the medium-F biotite granites to the high-F, high-P_2O_5 Li-mica granites and alkali-feldspar syenites.

(b) Analyzed monazite grains from the Krudum granite body display strong preference of cheralite substitution over the huttonite substitution with up to 69.3 mol % cheralite component in the alkali-feldspar syenites. Some monazite grains from the alkali-feldspar syenites are enriched in ThO_2 (up to 35.4 wt % ThO_2).

(c) The coupled thorite-coffinite and cheralite substitutions are dominant in the analyzed xenotime. Some xenotime analyses reveal low totals, suggesting probably their hydrothermal alteration.

(d) Zircon grains from these granites are sometimes metamictized and fluorized. Zircon from the high-F, high-P_2O_5 Li-mica granites and alkali-feldspar syenites is usually enriched in P (up to 8.29 wt % P_2O_5; 0.24 apfu P). The higher concentrations of P, Y, REE and Sc returned by zircon grains from the high-F, high-P_2O_5 Li-mica granites could be explained by their metamictization. However, the highest concentration of P (8.29 wt % P_2O_5; 0.24 apfu P) that was found in zircon grains from alkali-feldspar syenite without visible metamictization could be believed as the result of a primary magmatic enrichment produced by fractionation.

Acknowledgments: The research for this paper was carried out thanks to the support of the long-term conceptual development research organization RVO 67985891. P. Gadas and R. Škoda from the Masaryk University, Brno are thanked for their assistance during the microprobe work. I wish also to thank A. Szameitat for her constructive remarks and English corrections. I am also grateful to three anonymous reviewers for numerous helpful comments and recommendations that helped to improve this paper.

Conflicts of Interest: The author declares no conflict of interest.

References

1. Bea, F. Residence of REE, Y, Th and U in granites and crustal protoliths; Implications for the chemistry of crustal melts. *J. Petrol.* **1996**, *37*, 521–552. [CrossRef]
2. Broska, I.; Petrík, I. Genesis and stability of accessory phosphates in silicic magmatic rocks: A Western Carpathian case study. *Mineralogia* **2008**, *39*, 53–65. [CrossRef]
3. Förster, H.J.; Rhede, D.; Hecht, L. Chemical composition of radioactive accessory minerals: Implications for the evolution, alteration, age, and uranium fertility of the Fichtelgebirge granites (NE Bavaria, Germany). *Neues Jahrbuch für Mineralogie* **2008**, *185*, 161–182. [CrossRef]
4. Harlov, D.E.; Procházka, V.; Förster, H.J.; Matějka, D. Origin of monazite-xenotime-zircon-fluorapatite assemblages in the peraluminous Melechov granite massif, Czech Republic. *Mineral. Petrol.* **2008**, *94*, 9–26. [CrossRef]
5. Hetherington, C.J.; Jercinovic, M.J.; Williams, M.L.; Mahan, K. Understanding geologic processes with xenotime: Composition, chronology, and a protocol for electron probe microanalysis. *Chem. Geol.* **2008**, *254*, 133–147. [CrossRef]
6. Kelts, A.B.; Ren, M.; Anthony, E.Y. Monazite occurrence, chemistry, and chronology in the granitoid rocks of the Lachlan Fold Belt, Australia: An electron microprobe study. *Am. Mineral.* **2008**, *93*, 373–383. [CrossRef]
7. Pérez-Soba, C.; Villaseca, C.; Orejana, D.; Jeffries, T. Uranium-rich accessory minerals in the peraluminous and perphosphorous Belvís de Monroy pluton (Iberian Variscan belt). *Contrib. Mineral. Petrol.* **2014**, *167*. [CrossRef]
8. Uher, P.; Kohút, M.; Ondrejka, M.; Konečný, P.; Siman, P. Monazite-(Ce) in Hercynian granites and pegmatites of the Bratislava massif, Western Carpathians: Compositional variations and Th-U-Pb electron-microprobe dating. *Acta Geol. Slov.* **2014**, *6*, 215–231.

9. Breiter, K. Monazite and zircon as major carriers of Th, U, and Y in peraluminous granites: Examples from the Bohemian Massif. *Mineral. Petrol.* **2016**, *110*, 767–785. [CrossRef]
10. Förster, H.J.; Tischendorf, G.; Trumbull, R.B.; Gottesmann, B. Late-collisional granites in the Variscan Erzgebirge (Germany). *J. Petrol.* **1999**, *40*, 1613–1645. [CrossRef]
11. Förster, H.J.; Romer, R.L. Carboniterous magmatism. In *Pre-Mesozoic Geology of Saxo-Thuringia—From the Cadomian Active Margin to the Variscan Orogen*; Linnemann, U., Romer, R.L., Eds.; Schweizerbart Verlag: Stuttgart, Germany, 2010; pp. 287–308.
12. Blecha, V.; Štemprok, M. Petrochemical and geochemical characteristics of late Variscan granites in the Karlovy Vary Massif (Czech Republic)–implications for gravity and magnetic interpretation at shallow depths. *J. Geosci.* **2012**, *57*, 65–85. [CrossRef]
13. Hofmann, Y.; Jahr, T.; Jentzch, G. Three-dimensional gravimetric modelling to detect deep structure of the region Vogtland/NW Bohemia. *J. Geodyn.* **2003**, *35*, 209–220. [CrossRef]
14. Finger, F.; Gerdes, A.; René, M.; Riegler, G. The Saxo-Danubian granite belt: Magmatic response to post-collisional delamination of mantle lithosphere below the south-western sector of the Bohemian Massif (Variscan orogen). *Geol. Carpath.* **2009**, *60*, 205–212. [CrossRef]
15. Tichomirova, M.; Leonhardt, D. New age determinations (Pb-Pb zircon evaporation, Rb/Sr) on the granites from Aue-Schwarzenberg and Eibenstock, Western Erzgebirge, Germany. *Z. Geol. Wiss.* **2010**, *38*, 99–123.
16. Dolejš, D.; Bendl, J.; Štemprok, M. Rb-Sr isotopic composition in the Western Krušné hory/Erzgebirge pluton, Central Europe: Record of variations in source lithology, mafic magma input and postmagmatic hydrothermal events. *Mineral. Petrol.* **2016**, *110*, 601–622. [CrossRef]
17. Machek, M.; Roxerová, Z.; Janoušek, V.; Petrovský, E.; René, M. Petrophysical and geochemical constraints on alteration processes in granites. *Stud. Geophys. Geodaet.* **2013**, *57*, 710–740. [CrossRef]
18. Breiter, K.; Förster, H.J.; Seltmann, R. Variscan silicic magmatism and related tin-tungsten mineralization on the Erzgebirge-Slavkovský les metallogenic province. *Miner. Depos.* **1999**, *34*, 505–521. [CrossRef]
19. Jarchovský, T. The nature and genesis of greisen stocks at Krásno, Slavkovský les area–western Bohemian, Czech Republic. *J. Czech Geol. Soc.* **2006**, *51*, 201–216.
20. René, M.; Škoda, R. Nb-Ta-Ti oxides fractionation in rare-metal granites: Krásno-Horní Slavkov ore district, Czech Republic. *Mineral. Petrol.* **2011**, *103*, 37–48. [CrossRef]
21. Dolníček, Z.; René, M.; Prochaska, W.; Kovář, M. Fluid evolution of the Hub stock, Horní Slavkov-Krásno Sn-W ore district, Bohemian Massif, Czech Republic. *Miner. Depos.* **2012**, *47*, 821–833. [CrossRef]
22. René, M. Petrology, geochemistry and mineralogy of greisens associated with tin-tungsten mineralisation: Hub stock deposit at Krásno-Horní Slavkov ore district, Czech Republic. In *Contributions to Mineralisation*; Al-Juboury, A.I., Ed.; InTech: Rijeka, Croatia, 2018; pp. 1–22.
23. Pouchou, J.L.; Pichoir, F. "PAP" (φ-ρ-Z) procedure for improved quantitative microanalysis. In *Microbeam Analysis*; Armstrong, J.T., Ed.; San Francisco Press: San Francisco, CA, USA, 1985; pp. 104–106.
24. Pyle, J.M.; Spear, M.S.; Rudnick, R.L.; McDonough, W.F. Monazite-xenotime-garnet equilibrium in metapelites and a new monazite-garnet thermometer. *J. Petrol.* **2001**, *42*, 2083–2107. [CrossRef]
25. Chappell, B.W.; Hine, R. The Cornubian batholith: An example of magmatic fractionation on a crustal scale. *Res. Geol.* **2006**, *56*, 203–244. [CrossRef]
26. Boynton, W.V. Geochemistry of the rare earth elements: Meteorite studies. In *Rare Earth Elements*; Henderson, P., Ed.; Elsevier: Amsterdam, The Netherlands, 1984; pp. 63–114.
27. Förster, H.J. The chemical composition of REE-Y-Th-U-rich accessory minerals in peraluminous granites of the Erzgebirge-Fichtelgebirge region, Germany. Part I: The monazite-(Ce)-brabantite solid solutions series. *Am. Mineral.* **1998**, *83*, 259–272. [CrossRef]
28. Hoshino, M.; Watanabe, Y.; Ishihara, S. Crystal chemistry of monazite from the granitic rocks of Japan: Petrogenetic implications. *Can. Mineral.* **2012**, *50*, 1331–1346. [CrossRef]
29. Gramaccioli, C.M.; Segalstad, T.V. A uranium- and thorium-rich monazite from a south-alpine pegmatite at Piona, Italy. *Am. Mineral.* **1978**, *63*, 757–761.
30. Franz, G.; Andrehs, G.; Rhede, D. Crystal chemistry of monazite and xenotime from Saxothuringian-Moldanubian metapelites, NE Bavaria, Germany. *Eur. J. Min.* **1996**, *8*, 1097–1118. [CrossRef]
31. Linthout, K. Tripartite division of the system $2REEPO_4$-$CaTh(PO_4)_2$-$2ThSiO_4$, discreditation of brabantite, and recognition of cheralite as a name for members dominated by $CaTh(PO_4)_2$. *Can. Mineral.* **2007**, *45*, 503–508. [CrossRef]

32. Förster, H.J. The chemical composition of REE-Y-Th-U-rich accessory minerals in peraluminous granites of the Erzgebirge-Fichtelgebirge region, Germany. Part II: Xenotime. *Am. Mineral.* **1998**, *83*, 1302–1315. [CrossRef]
33. Breiter, K.; Förster, H.J.; Škoda, R. Extreme P-. Bi-, Nb-, Sc-, U- and F-rich zircon from fractionated perphosphorus granites: The peraluminous Podlesí granite system, Czech Republic. *Lithos* **2006**, *88*, 15–34. [CrossRef]
34. Huang, X.; Wang, R.C.; Chen, X.M.; Hu, H.; Liu, C.S. Vasrtical variations in the mineralogy of the Yichun topaz-lepidolite granit, Jiangxi province, Southern China. *Can. Mineral.* **2002**, *40*, 1047–1068. [CrossRef]
35. Uher, P. Accessory zircon in orogenic to post-orogenic granites and pegmatites: Compositional variations as indicator of magmatic evolution. An example from western Carpathian, Slovakia. *Geophys. Res. Abstr.* **2005**, *7*, 09440.
36. Breiter, K.; Škoda, R. Vertical zonality of fractionated granite plutons reflected in zircon chemistry: The Cínovec A-type versus the Beauvoir S-type granite suite. *Geol. Carpath.* **2012**, *63*, 383–398. [CrossRef]
37. Förster, H.J. Composition and origin of intermediate solid solutions in the system thorite-xenotime-zircon-coffinite. *Lithos* **2006**, *88*, 35–55. [CrossRef]
38. Hata, S. Xenotime and variety of zircon from Iisaka. *Sci. Pap. Inst. Chem. Res.* **1938**, *34*, 619–622.
39. Uher, P.; Černý, P. Zircon in Hercynian granitic pegmatites of the Western Carpathians, Slovakia. *Geol. Carpath.* **1998**, *49*, 261–270.
40. Hoskin, P.W.O.; Kinny, P.D.; Wyborn, D.; Chappell, B.W. Identifying accessory mineral saturation during differentiation in granitoid magmas: An integrated approach. *J. Petrol.* **2000**, *41*, 1365–1396. [CrossRef]
41. Finch, R.J.; Hanchar, J.M. Structure and chemistry of zircon and zircon group minerals. *Rev. Mineral. Geochem.* **2003**, *53*, 1–26. [CrossRef]
42. Bernhard, F.; Walter, F.; Ettinger, K.; Taucher, J.; Mereiter, K. Pretulite, $ScPO_4$: A new scandium mineral from the Styrian and lower Austrian lazulite occurrences, Austria. *Am. Mineral.* **1998**, *83*, 625–630. [CrossRef]
43. Geisler, T.; Rashwan, A.A.; Rahn, A.K.; Poller, U.; Zwingmann, H.; Pidgeon, R.T.; Schleicher, H.; Tolmaschek, F. Low-temperature hydrothermal alteration of natural metamict zircons from the Eastern Desert Egypt. *Mineral. Mag.* **2003**, *67*, 485–508. [CrossRef]
44. Nasdala, L.; Pidgeon, R.T.; Wolf, D. Heterogeneous metamictization of zircon on a microscale. *Geochem. Cosmochim. Acta* **1996**, *60*, 1091–1097. [CrossRef]
45. Nasdala, L.; Kronz, A.; Wirth, R.; Vászi, T.; Pérez-Soba, C.; Willner, A.; Kennedy, A.K. The phenomenon of different electron microprobe totals in radiation-damaged and altered zircon. *Geochim. Cosmochim. Acta* **2009**, *73*, 1637–1650. [CrossRef]
46. René, M. Composition of coexisting zircon and xenotime in rare-metal granites from the Krušné Hory/Erzgebirge Mts. (Saxothuringian Zone, Bohemian Massif). *Miner. Petrol.* **2014**, *108*, 551–569. [CrossRef]
47. Johan, Z.; Johan, V. Accessory minerals of the Cínovec (Zinnwald) granite cupola, Czech Republic. Part 1: Nb-, Ta- and Ti-bearing oxides. *Mineral. Petrol.* **2005**, *83*, 113–150. [CrossRef]
48. Förster, H.J.; Rhede, D. The Be-Th-rich granite of Seiffen (eastern Erzgebirge, Germany): Accessory-mineral chemistry, composition, and age of late-Variscan Li-F granite of A-type affinity. *Neues Jahrbuch für Mineralogie* **2006**, *182*, 307–321. [CrossRef]
49. Pointer, C.M.; Ashworth, J.R.; Ixer, R.A. The zircon-thorite mineral group in metasomatized granite, Ririwai, Nigeria 1. Geochemistry and metastable solid solution in thorite and coffinite. *Mineral. Petrol.* **1988**, *38*, 245–262. [CrossRef]
50. Smith, D.G.W.; De St, J.L.; Reed, S.J.B.; Long, J.V.P. Zonally metamictized and other zircon from Thor Lake, Northwest Territories. *Can. Mineral.* **1991**, *29*, 301–309.
51. Peréz-Soba, C.; Villaseca, C.; Gonzáles del Tánago, J. The composition of zircon in the peraluminous Hercynian granites of the Spanish Central System batholith. *Can. Mineral.* **2007**, *45*, 509–527. [CrossRef]
52. Anderson, A.J.; Wirth, R.; Thomas, R. The alteration of metamict zircon and its role in the remobilization of high-field-strength elements in the Georgeville granite, Nova Scotia. *Can. Mineral.* **2008**, *46*, 1–18. [CrossRef]

53. Abd El-Naby, H.H. High and low temperature alteration of uranium and thorium minerals, Um Ara granites, south Eastern Desert, Egypt. *Ore Geol. Rev.* **2009**, *35*, 436–446. [CrossRef]
54. Hoshino, M.; Kimata, M.; Nishida, N.; Shimizu, M.; Akasaka, T. Crystal chemistry of zircon from granitic rocks, Japan: Genetic implications of HREE, U and Th enrichment. *Neues Jahrbuch für Mineralogie* **2010**, *187*, 167–188. [CrossRef]